energies

MDPI

Article

A Novel Method for On-Line Characterization of Alkali Release and Thermal Stability of Materials Used in Thermochemical Conversion Processes

Viktor Andersson, Yaxin Ge, Xiangrui Kong and Jan B. C. Pettersson *

Department of Chemistry and Molecular Biology, University of Gothenburg, 41296 Gothenburg, Sweden; viktor.andersson@cmb.gu.se (V.A.); yaxin.ge@gu.se (Y.G.); xiangrui.kong@chem.gu.se (X.K.)
* Correspondence: janp@chem.gu.se

Abstract: Alkali metal compounds are released during the thermal conversion of biofuels and fossil fuels and have a major impact on the efficiency of conversion processes. Herein, we describe a novel method for the simultaneous characterization of alkali release and mass loss from materials used in combustion and gasification processes including solid fuels, fluidized bed materials, and catalysts for gas reforming. The method combines the thermogravimetric analysis of selected samples with the on-line measurement of alkali release using a surface ionization detector. The technique builds on the careful treatment of alkali processes during transport from a sample to the downstream alkali monitor including the losses of alkali in the molecular form to hot walls, the formation of nanometer-sized alkali-containing particles during the cooling of exhaust gases, aerosol particle growth, and diffusion losses in sampling tubes. The performance of the setup was demonstrated using biomass samples and fluidized bed material from an industrial process. The emissions of alkali compounds during sample heating and isothermal conditions were determined and related to the simultaneous thermogravimetric analysis. The methodology was concluded to provide new evidence regarding the behavior of alkali in key processes including biomass pyrolysis and gasification and ash interactions with fluidized beds. The implications and further improvements of the technique are discussed.

Keywords: TGA; surface ionization; potassium; sodium; ilmenite; biomass

Citation: Andersson, V.; Ge, Y.; Kong, X.; Pettersson, J.B.C. A Novel Method for On-Line Characterization of Alkali Release and Thermal Stability of Materials Used in Thermochemical Conversion Processes. *Energies* **2022**, *15*, 4365. https://doi.org/10.3390/en15124365

Academic Editor: Albert Ratner

Received: 24 May 2022
Accepted: 14 June 2022
Published: 15 June 2022

1. Introduction

Biomass and solid fossil fuels are commonly used to generate heat and electricity by combustion and to produce chemicals such as hydrogen, synthesis gas, and bio-oil by pyrolysis and gasification [1]. The further development of the various processes is driven by several factors including the need to improve the efficiency, increase versatility and fuel flexibility, and reduce the environmental and climate impact, which all benefit from a detailed understanding of the underlying physicochemical processes.

The thermal conversion of a fuel is a relatively complex process with several inherent challenges. Some of the challenges are associated with the presence of condensable material in the gas product. One important category is alkali metal compounds that are released during thermal conversion [2,3]. Biomass is rich in potassium and sodium compounds [3], and coal may also contain high concentrations of alkali, in particular, sodium, depending on the origin of the fuel [4]. In the following, we will interchangeably refer to potassium- and sodium-containing compounds as alkali, alkali compounds, or alkali metal compounds.

Several compounds including KOH and KCl are readily released to the gas phase during the thermal conversion of a fuel. Gaseous alkali compounds interact with available surfaces in the hot environment and are well-known to have a major influence on the efficiency of conversion processes. Some common issues are related to alkali interactions with the bed material in fluidized beds [5–8]. Alkali contributes to the formation of ash

layers on the bed particles, which may result in the formation of melted ad-layers and an increased risk of bed agglomeration [7,9]. Alkali interactions with fluidized bed materials may also change their function in other ways (e.g., alkali uptake on oxygen carriers in chemical looping combustion may affect their reactivity, oxygen carrying ability, lifetime or cause particle agglomeration) [6,7,9–12].

Most alkali compounds re-condense as temperatures drop below 500–600 °C and fouling and corrosion of the system equipment and heat extraction units are major issues induced by alkali compounds in gaseous or particulate forms [2,13]. Alkalis may also influence other downstream components including catalysts used for gas reforming [14]. Alkali metals are commonly used as promoters in catalytic processes, and changing the concentrations may modify their function and shift conditions from the optimum. Another example of affected downstream equipment includes gas turbines, which may be sensitive to corrosion and deposits already at relatively low alkali concentrations [2]. In contrast to these concerns, alkalis may also be catalytically active and have positive effects on tar cracking [15] and char reactivity [16].

These examples emphasize the need for a detailed understanding of alkali interactions with materials present in the high temperature environment of a thermal conversion process. Alkali is, in general, known to be relatively mobile under process conditions and may be found in both gaseous and condensed forms at high temperatures. Ideally, alkali interactions with other components present in the high temperature environment should be sufficiently well-known to predict the influence of temperature, gas composition, and the condensed materials present. Examples of the relevant condensed materials include fluidized bed particles, ash, char, reactor walls, surfaces of cleaning devices, and catalysts.

Several techniques have been applied to characterize the alkali processes in systems ranging from the laboratory to the industrial scale. Available alkali measurement systems can be divided into off-line and on-line methods. Off-line systems extract samples for subsequent analysis and a large number of methods are used to provide valuable information about the concentration and distribution of alkali and other elements in the samples; one example being scanning electron microscopy with energy dispersive spectroscopy [6,10,17]. On-line measurements are either based on in situ measurements or continuous gas extraction and have been performed using several methods including surface ionization methods [5,13,18–20], mass spectrometry [21], excimer laser induced fragmentation [22], and tunable diode laser absorption spectroscopy [23]. Gas extraction is challenging since alkali compounds will condense on any available surfaces when the gas is quenched and cooled including walls in the extraction system and other existing aerosol particles [18,20,24]. In practice, the total surface of aerosol particles including both the existing particles and particles formed by nucleation, often dominates over the wall surface area and losses to the walls are limited. In addition, experiments in laboratory reactors may often be more challenging than pilot or industrial scale studies due to a larger surface-to-volume ratio in small setups [5,20]. Considering these different difficulties, there is a remaining need for reliable and practical methods for the systematic characterization of alkali interactions with high temperature materials.

Here, we present a novel laboratory method for the simultaneous characterization of alkali release and mass loss from materials used in thermal conversion processes. The method combines the thermogravimetric analysis (TGA) of samples with the on-line measurement of alkali release using a surface ionization detector (SID) [13,18,19]. The high sensitivity of the SID allows for time-resolved monitoring of alkali emissions from the relatively small samples (mg range) used in a TGA. Both techniques are well-established independently, but their combination requires careful consideration to provide reliable results. As described above, alkali compounds will interact with any existing surfaces in a thermal conversion process, and the same is true within the TGA-SID setup. We present the results from the laboratory and modeling studies with the aim to characterize the role of key processes including the loss of alkali in molecular form to hot walls, and the behavior of nanometer-sized alkali-containing particles formed by nucleation during the cooling of

the exhaust gas from the TGA. We also demonstrate the use of the new TGA-SID setup with the biomass samples and fluidized bed material from an industrial process, and related the emissions of alkali compounds to the thermal stability of the investigated samples. The implications and potential further improvements of the technique are discussed.

2. Methodology

2.1. Experimental Setup

The employed experimental setup consists of a commercial TGA (Model Q500, TA Instruments Inc., New Castle, DE, USA) connected to a SID, and the setup is schematically shown in Figure 1. The system allows for the on-line measurements of alkali, leaving a sample at a certain temperature while the sample weight is continuously monitored. Related earlier methods include techniques for the determination of alkali release during the heating of samples (without sample mass monitoring) [25] and the characterization of alkali release and sample mass at high heating rates [26].

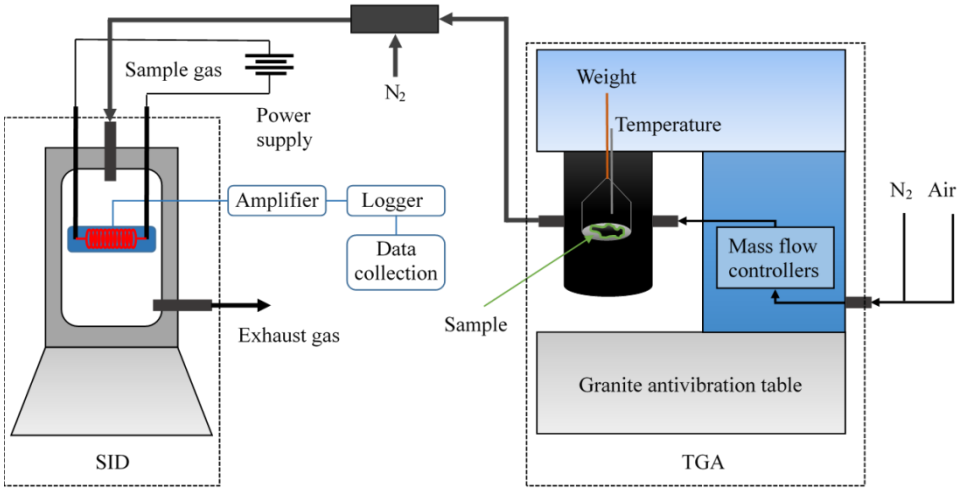

Figure 1. The experimental TGA-SID setup used for the simultaneous characterization of alkali release and mass loss from a selected sample. The main components of the SID are a hot Pt filament (coiled wire marked in red) and a nearby ion collector plate (blue area behind red wire); see text for the details.

The TGA was operated with a constant flow of 10 mL min^{-1} N_2 protective balance gas and 90 mL min^{-1} of either inert (N_2) or oxidizing (synthetic air) purge gas. Reducing gases were available as an alternative, but not used in the present study. The gas flows across the sample, which was spread on a 100 µL platinum crucible shaped like an 11 mm wide disc with a 1 mm wall around the edge. A comparison between the platinum and alumina crucibles showed that the former produced a lower alkali background in the experiments. Samples with a mass between 0.5 and 20 mg could be used, and the heating and cooling rates, the duration of periods with isothermal conditions, and gas selection were defined by the user. The maximum heating and cooling rates were 20 °C min^{-1} and the maximum temperature was 1000 °C.

2.2. Alkali Detection Method

The SID instrument has been presented in detail elsewhere [27,28], and has been successfully applied in thermal conversion studies on a laboratory scale [5,20], pilot scale [13,29], and industrial scale [19,30]. The technique is based on a natural phenomenon known as surface ionization where atoms thermally desorb in ionic form from a metal surface [27,28]. The ionization potential (IP) of most atoms and molecules is higher than the work function (ϕ) of a metal surface, which favors the emission of neutral species while desorption in the ionic form can safely be ignored [31]. The alkali metals have unusually low IPs compared to ϕ, which enables ion desorption [27], and potassium and sodium

typically have ionization probabilities of >99% and 89%, respectively, on a hot platinum surface [31]. Although other alkali metals also have high ionization probabilities, they are considerably less abundant in thermal conversion applications and can be neglected. Some alkaline earth metals (Sr and Ba) also have a high probability to desorb in ionic form, but their binding energies to platinum are significantly higher and their desorption rates are negligible at the operation temperature of the SID [31]. As a consequence of the above, the SID has a very high sensitivity and selectivity for Na and K, which is a requirement for the present application.

Alkali species leaving a sample in the TGA are transported with the exhaust gases and fed into the SID system (Figure 1). The exhaust gas was diluted with 600 mL min^{-1} N_2 before entering the SID in order to comply with a requirement of a total flow of 700 mL min^{-1} for the instrument. The SID consists of two key components: a hot platinum filament and a nearby ion collector plate (Figure 1). The filament is a 0.3 mm diameter platinum wire that is resistively heated to 1400 K while being kept at 300 V. The ion collector is a grounded metal plate, located a few millimeters from the filament. When an alkali-containing gas flows through the SID compartment, alkali compounds will impact and dissociate on the filament and subsequently desorb as alkali ions. The positively charged alkali ions diffuse from the positively charged filament to the grounded collector plate where they give rise to a current that is amplified and measured.

The SID used in this study detects the total alkali (K + Na) concentration in a sample flow with a time resolution of 1 s. The current measured with the SID was transformed into an alkali mass concentration by a separate calibration experiment. A continuous flow of KCl aerosol particles was generated with an aerosol atomizer (Model 3076, TSI Inc., Shoreview, MN, USA), and fed in parallel to the SID and a scanning mobility particle sizer (SMPS) (see schematic overview in Figure S1 in the Supplementary Materials). The SMPS (Model 3936, TSI Inc., Shoreview, MN, USA) measures the aerosol particle number concentration as a function of particle size in a gas flow, and the mass concentration of alkali aerosol particles in the gas suspension is calculated assuming spherical particles with a constant particle density. Dried pure KCl particles are not expected to be spherical, but the procedure was considered to be sufficient for the present purpose. The results from the calibration, where the KCl concentration was converted to K concentration and the SID background signal was subtracted, are presented in Figure 2 and Equation (1):

$$[\mathrm{K}]\left(\mu\mathrm{g\ m^{-3}}\right) = \frac{\text{SID signal (nA)}}{0.0466} \quad (1)$$

and indicate a linear relationship between the SID signal and the KCl mass concentration determined by the SMPS.

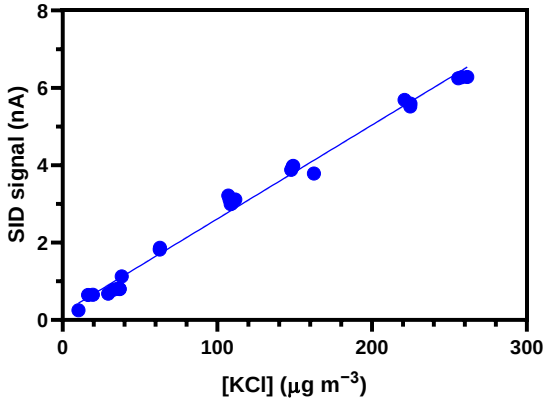

Figure 2. The signal measured by the SID as a function of mass concentration of K (µg m^{-3}) based on the concentration of KCl aerosol particles determined by a SMPS. The calibration experiments were carried out using a continuous flow of KCl aerosol particles generated with an aerosol atomizer (see the text for details).

2.3. Samples Used for Method Evaluation and Demonstration

Experiments with known amounts of pure alkali species were conducted in the TGA-SID system in order to estimate the losses of alkali between the sample holder in the TGA and the SID unit. This was conducted by mixing known amounts of KCl or NaCl in pure water and adding a drop of the solution to the TGA sample holder. The water was allowed to evaporate at low temperature, leaving a layer of dried alkali salt on the sample holder. As the temperature increased, the salt evaporated and the integrated amount of alkali detected by the SID was compared with the amount of salt placed in the TGA.

Biomass samples were used to demonstrate the instrument performance with a typical biofuel. The biomass consisted of pine pellets with an original size of 1.5–2 mm. The pellets were ground and sieved to obtain a pine powder with an average particle size less than 0.3 mm. Ultimate and proximate analyses of the samples showed that they had a typical composition for softwood including an ash content of 16%. The mineral content was determined with inductively coupled plasma atomic emission spectroscopy (ICP-OES). Potassium was relatively abundant in the sample (0.048 wt%, dry weight), and other elements had typical concentrations for the fuel type including Na (0.004 wt%), Ca (0.094 wt%), and Si (0.019 wt%).

Samples of ilmenite ($FeTiO_3$) oxygen carrier particles were used in the experimental evaluation of alkali release from the fluidized bed material. The samples were obtained from an industrial 115 MW_{th} circulating fluidized bed boiler that was operated in oxidizing conditions at 850 °C using a biofuel mixture of 50:50 wood chips and recovered waste wood [32]. Bottom ash samples were extracted after 225 h of operation before being sieved and magnetically separated to obtain an ilmenite-rich fraction [17]. Analysis of the elemental composition showed that the accumulation of ash elements had occurred, with sample K and Na mass concentrations of approximately 2% and 1%, respectively. Sieving analysis was performed on the particles and a mean surface diameter of 146 µm was determined. A small magnet was used to collect a fraction of the sample, and 13 mg was placed on the TGA sample holder.

3. Results

We first present the results from experiments with known amounts of alkali salts in the TGA, followed by an analysis regarding the influence of the formation of alkali-containing aerosol particles during the cooling of the exhaust gases, modeling of alkali losses to hot walls in the TGA, and finally, the demonstration of the method using biomass and fluidized bed samples.

3.1. Experiments with Pure Alkali Salts

The results from the experiments with known amounts of pure alkali salts in the TGA are presented in Figure 3. The experiments were carried out by placing a water droplet with a known volume and alkali chloride concentration on the Pt sample holder, and the temperature was then increased from room temperature to 1000 °C with 20 °C min^{-1}. The water droplet rapidly evaporated and the remaining salt desorbed at temperatures above 500 °C, and the displayed alkali values were integrated values during the complete temperature ramp. Linear relationships were observed between the integrated amount of alkali measured by the SID and the amount in the TGA. The losses varied between 53 and 84% for all experiments, with generally higher losses observed when low amounts were used. The average amount of alkali measured by the SID compared to the amount of alkali placed in the TGA was 26% for KCl and 39% for NaCl. The observed differences between the two salts could have multiple reasons including a difference in their interaction with the Pt crucible, which may become more important in this special case with pure alkali salts compared to more realistic samples.

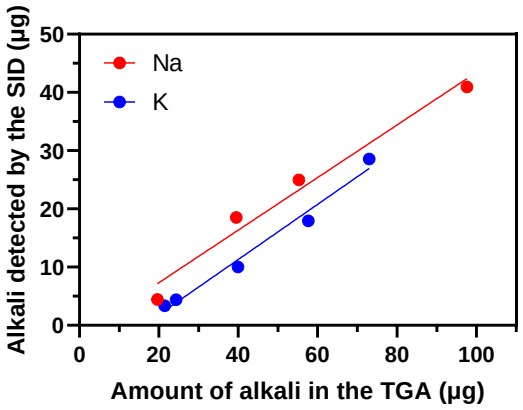

Figure 3. The integrated amount of alkali detected by the SID as a function of the amount of K or Na used in the TGA.

The used alkali salt samples were in the 40–250 µg range and the samples were considerably smaller than the typical sample weights used in the TGA (mg range). The observed alkali emission was, however, substantially larger for the pure salts since most relevant samples from high temperature conversion processes contained low or very low concentrations of alkali. For example, the amount of alkali leaving the TGA in the ilmenite study presented below (Section 3.4) was approximately two orders of magnitude lower than that used in the pure salt experiments.

3.2. Losses in Sampling Lines between the TGA and the SID

We next evaluated the importance of losses in the cold sampling lines between the TGA and the SID. When the gaseous alkali species left the hot TGA and entered the cold exhaust lines, they will rapidly nucleate to form nanometer-sized aerosol particles. These aerosol particles were dispersed in the 100 mL min^{-1} gas flow, leaving the TGA and passed through a metal tube of stainless steel with an inner diameter of 2 mm before entering a diluter. After the diluter, the aerosol particles were dispersed in a 700 mL min^{-1} gas flow and transported to the SID in a rubber tube with an inner diameter of 6 mm. After initial quenching of the hot gas, the sampling lines were kept at room temperature to minimize the thermophoretic forces and associated particle losses.

To estimate the losses of the nanometer-sized aerosol particles to the tube walls, experiments were carried out where the length of the exhaust tubes was varied. The metal tube connecting the TGA to the diluter was varied between 7 and 31 cm, and the rubber tube connecting the diluter to the SID was varied between 21 and 90 cm. Tube lengths of 18 cm for the metal tube and 21 cm for the rubber tube were considered as standard cases. The effect of the exhaust tube length was studied during experiments with a 13 mg ilmenite sample at 1000 °C in an inert atmosphere.

The observed alkali transmission as a function of tube length of the metal and rubber tubes is shown in Figure 4. The displayed values are the relative values compared to the transmission when using a standard 18 cm metal tube and a 21 cm rubber tube, respectively. The alkali transmission substantially increases with the decreasing length of the metal tube, and the alkali transmission will be 2.4 times higher than the standard case if the line in Figure 4 is extrapolated to the zero tube length. A similar but less pronounced trend was observed when the length of the rubber tube was changed, and the extrapolation to the zero tube length increased the transmission 1.3 times compared to the standard case. If both tubes are simultaneously reduced to zero length, the alkali signal will be 3.2 times higher than that observed for the standard cases.

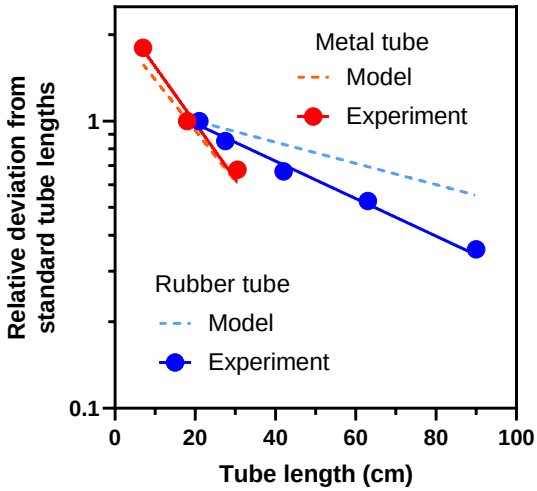

Figure 4. The relative alkali transmission through tubes connecting the TGA and the SID as a function of tube length: metal tube (red symbols and line) and rubber tube (blue symbols and line). Results obtained using a model for particle penetration through tubes [24] are included for the metal (orange dashed line) and rubber tube (light blue dashed line) cases.

The observed linear relationship between the alkali transmission on a logarithmic scale and tube length is consistent with diffusional particle losses in a laminar flow, which can be calculated with equations based on the empirical data [24]:

$$\begin{gathered} P = 1 - 5.50\mu^{\frac{2}{3}} + 3.77\mu \text{ for } \mu < 0.009 \\ P = 0.819\exp(-11.5\mu) + 0.0975\exp(-70.1\mu) \text{ for } \mu \geq 0.009 \end{gathered} \quad (2)$$

where P is the penetration of aerosol particles through a tube as a function of the dimensionless deposition parameter μ, calculated with the following equations [24]:

$$\mu = DL/Q \quad (3)$$

$$D = \frac{k_B T C_c}{3\pi\eta d_p} \quad (4)$$

$$C_c = 1 + \frac{\lambda}{d_p}\left[2.34 + 1.05xp\left(-0.39\frac{\lambda}{d_p}\right)\right] \quad (5)$$

where D (m^2 s^{-1}) is the diffusion coefficient for the aerosol particle; L (m) is the tube length; and Q (m^3 s^{-1}) is the volumetric flow rate of the sample gas. The diffusion coefficient is calculated from the Boltzmann constant k_B (m^2 kg s^{-2} K^{-1}), the temperature (K), the Cunningham correction factor C_c, the viscosity η (Pa s), and the particle diameter d_p (m). The dimensionless correction factor C_c is a function of the particle diameter and the mean free path λ (m).

In the present case, the particle diameter was calculated based on the alkali concentration detected by the SID in the ilmenite experiments and assuming spherical KCl particles with a particle number concentration of 5×10^8 cm^{-3} [24], which is a typical value for the number of particles formed by nucleation [24]. The results using the model are included in Figure 4. The model qualitatively describes the trends observed in the experiments, which confirms that particle losses can be understood based on well-established aerosol science concepts. The model was simplified compared to the actual conditions and no attempt was made to fit the experimental data. As can be seen in Equation (3), the deposition parameter μ depends on the volumetric flow rate of the sample gas. The flow rate in the rubber tube was six times higher compared to the flow rate in the metal tube. This explains why the alkali transmission changed significantly with the metal tube length, and to a smaller extent with the rubber tube length.

3.3. Loss of Alkali in Molecular Form to Hot Surfaces

Another potentially important source of alkali losses is the interactions of alkali in a molecular form with hot surfaces in the TGA compartment or gas outlet. Computational fluid dynamics (CFD) simulations were employed for the qualitative evaluation of temperature gradients and the gas flow profiles in the TGA quartz reactor. The CFD simulation was performed with the ANSYS Fluent 2021 R2 software, which is widely used in the CFD community [33–35], and the CFD methodology is described in detail in Section S2 in the Supplementary Materials.

Figure 5 shows the temperature and velocity profiles when the TGA is operated at a constant temperature of 1000 °C in air. The temperature profile in Figure 5a predicts that the sample holder reaches the target temperature of 1000 °C, and the quartz surface of the main TGA compartment and gas outlet had a temperature between 850 and 1000 °C. The velocity profiles in Figure 5b and Figure S2 in the Supplementary Materials show that the majority of the gas flowed over the sample before exiting through the outlet tube, without causing significant turbulence in the TGA compartment above and below the sample holder. Due to the low turbulence, we predict that the majority of the gas interactions with hot quartz surfaces will take place inside the outlet tube.

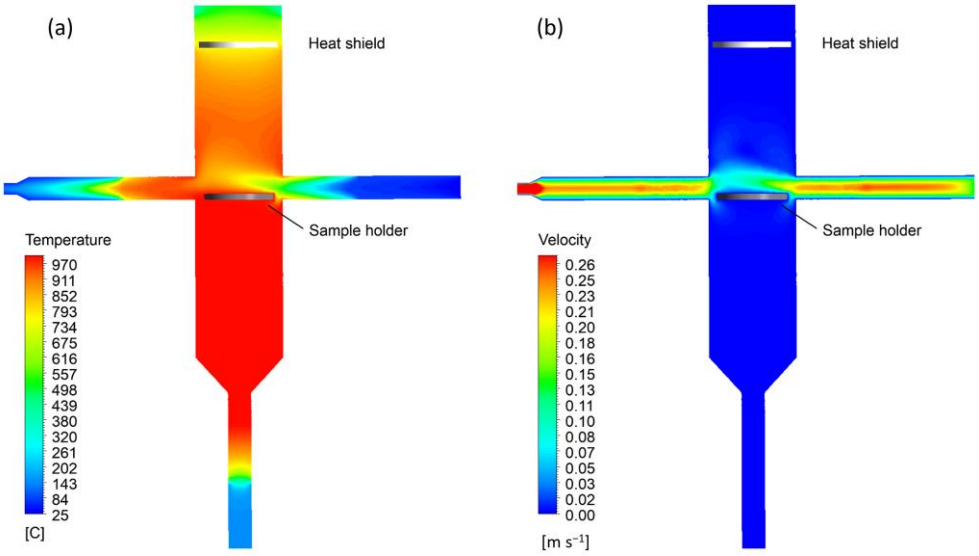

Figure 5. The results from the CFD simulations of the TGA when operated at a constant temperature of 1000 °C in air: (**a**) temperature profile and (**b**) velocity profile. The positions of the sample holder and a heat shield are indicated in the figure. The 11 mm wide sample holder can be used as a reference for the dimensions.

Gaseous alkali species leave the TGA through a hot quartz tube with a length of 3 cm and an inner diameter of 4 mm (to the left in Figure 5) before entering the colder exhaust tube lines. In this section, alkali compounds will be in the gas phase when the temperature is higher than approximately 500 °C [18,20]. Since gas molecules have large diffusion coefficients, a fraction of the alkali compounds will likely impact at the hot tube wall. The loss of alkali by molecular diffusion was calculated with a model for radial diffusion and the penetration of gas molecules and aerosol particles through laminar flow reactors, denuders, and sampling tubes developed by Knopf, Pöschl, and Shiraiwa (KPS method), according to the following equation [36]:

$$P_X = \exp\left(-\frac{\gamma_X}{1+3\gamma_X/\left(2N_{Shw}^{eff}Kn_X\right)}\frac{\omega_x}{D_{tube}}t\right) \quad (6)$$

where P_X is the penetration or transmission of molecules in a system. The case considered is KCl(g) diffusion in nitrogen carrier gas at 900 °C and the system properties and relevant parameters are listed in Table 1.

Table 1. A summary of the parameters applied in diffusion calculations for KCl in a nitrogen carrier gas at 900 °C. See [36] for a definition of the individual parameters.

T (K)	Temperature		1173.15
p (hPa)	Pressure		1013
Re	Reynolds number	$Re = \nu D_{tube}\rho/\eta$	12.05
Pe_X	Peclet number	$Pe_X = D_{tube}\nu_{g,X}/D_{g,X}$	93.09
λ_X (cm)	Mean free path	$\lambda_X = 3D_{g,X}/\omega_X$	1.18×10^{-5}
Kn_X	Knudsen number	$Kn_X = 2\lambda_X/D_{tube}$	6.41×10^{-5}
ω_X (cm·s^{-1})	Thermal molecular velocity	$\omega_X = \sqrt{\frac{8k_BT}{m\pi}}$	5.78×10^{4}
$\nu_{g,X}$ (cm·s^{-1})	Flow velocity		53.05
$D_{g,X}$ (cm^2·s^{-1})	Self-diffusion coefficient		0.23
t (s)	Residence time		0.06
D_{tube} (cm)	Tube diameter		0.40
l_{tube} (cm)	Tube length		3.00
z^*	Dimensionless axial distance	$z^* = z\left(\frac{\pi}{2}\right)\left(\frac{D_{g,X}}{Q}\right),\ z \leq l_{tube}$	0.16
γ_X	Uptake coefficient		1.00
$N_{shw}{}^{eff}$	Effective Sherwood number	$N_{Shw}^{eff} = 3.6568 + \frac{0.0978}{z^* + 0.0154}$	4.17
Q (m^3·s^{-1})	Flow rate		6.56×10^{-6}
η (kg·m^{-1}s^{-1})	Dynamic viscosity nitrogen		4.40×10^{-5}
ρ (kg·m^{-3})	Density nitrogen		0.25
m (kg)	Mass		1.23×10^{-25}
k_B (m^2 kg s^{-2}K^{-1})	Boltzmann's constant		1.38×10^{-23}

A self-diffusion coefficient D of 0.0256 cm^2 s^{-1} for KCl(g) in an ambient atmosphere was calculated based on known values for other gases and assuming a linear relationship between the self-diffusion coefficient and the molecular mass [37]. Furthermore, the self-diffusion coefficient was adjusted for the high temperature used here according to [38]:

$$D \propto \frac{T^{\frac{3}{2}}}{p} \tag{7}$$

where p is pressure, which resulted in D = 0.23 cm^2 s^{-1} for KCl(g) at 900 °C.

Based on the employed KPS method, the transmission of KCl molecules in the hot section of the exhaust system was estimated to be 25% at 900 °C, assuming unity accommodation of the molecules reaching the wall and that the axial distance travelled by each molecule equals the total length of the tube.

There is a significant influence of the tube length on the alkali transmission, and for tube lengths of 2, 3, and 4 cm, the transmission would be 38, 25, and 17%, respectively. The transmission was less sensitive to temperature and varied between 24 and 28% in the 700–1000 °C range. The effect of temperature was less pronounced since some key parameters had opposing influences on the transmission. A temperature increase resulted in an increase in significant parameters such as the diffusion coefficient, whereas parameters such as the residence time in the tube were reduced due to a higher volumetric flow rate. The alkali uptake in this hot section of the TGA-SID setup was concluded to be substantial, which needs to be considered in the evaluation of the new method.

3.4. Characterization of Biomass and Fluidized Bed Samples Using TGA-SID

The performance of the new TGA-SID was evaluated using two types of samples, a softwood sample and a fluidized bed material used in an industrial application. Typical sample mass and alkali release results obtained during biomass pyrolysis in an inert atmosphere are illustrated in Figure 6. Duplicate experiments were carried out and all of the main features were reproduced with signals typically varying by less than 5% between experiments. An initial mass loss was observed below 100 °C and was associated with the evaporation of moisture [39–41]. As expected, no alkali release was observed in this temperature range. The mass loss rate and alkali release rate rose sharply as the temperature increased above 200 °C and both reached a maximum around 370 °C. The observed alkali release followed the mass loss data, which indicates that the kinetics for alkali emission are closely associated with the breakdown of the organic structure during pyrolysis, in agreement with the findings from earlier studies [25,26,42].

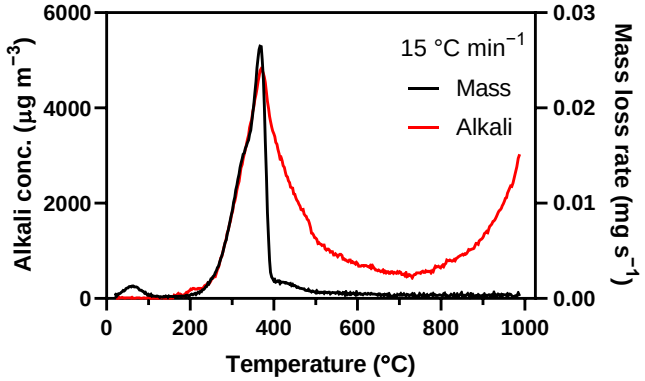

Figure 6. The mass loss rate (black line) and alkali concentration (red line) as a function of temperature during biomass pyrolysis in N_2 at a heating rate of 15 °C min^{-1}.

As the temperature was further increased, the mass loss dropped rapidly and the remaining loss was mainly attributed to the decomposition of more heat-resistant compounds and carbonaceous structures [39–41]. In contrast, the alkali release displayed a significantly different pattern above 370 °C. Although the alkali signal initially dropped, the emission remained relatively high and again increased above 700 °C, which is likely to be caused by inorganic alkali compounds in the remaining ash and char. It is concluded that the combined TGA and SID methods allow the mass loss and alkali release to be directly correlated, which may serve as a starting point for more detailed investigations of the underlying mechanisms responsible for the alkali kinetics.

Figure 7 shows the corresponding results for 13 mg samples of the ilmenite fluidized bed material. The samples had previously been used in a 115 MW_{th} power plant during an extended time period. The alkali results showed a substantial alkali peak between 630 and 800 °C in both the oxidizing and inert environments. Note that although the alkali peak was large, it was not associated with a substantial sample weight loss, which illustrates the high sensitivity of the SID. The peak likely originates from loosely bound alkali at the surface of the particles, which may have condensed while the samples were extracted from the hot environment in the power plant. As the temperature rose, a second alkali release started at around 900 °C and continued during the subsequent period with isothermal conditions.

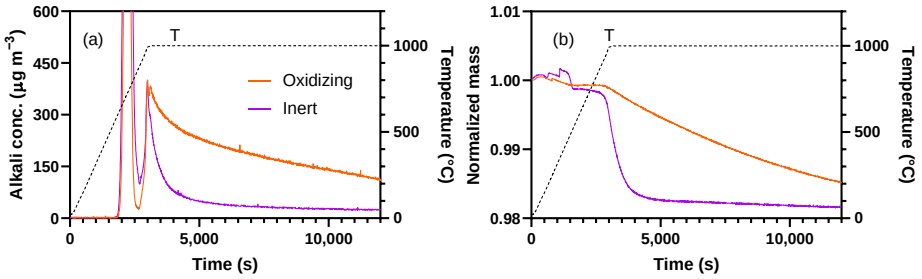

Figure 7. (**a**) The alkali desorption profiles and (**b**) mass loss profiles obtained in the experiments with an ilmenite oxygen carrier previously used for biomass combustion in a 115 MWth power plant. Experiments were carried out in inert and oxidizing atmospheres at a heating rate of 20 °C min^{-1} followed by an extended period at 1000 °C.

The total amount of alkali released by the ilmenite can be estimated by integrating the SID signal over time. The alkali released from the ilmenite samples corresponded to the 1.27 and 2.87 g kg^{-1} sample in the inert and oxidizing atmosphere, respectively. The alkali content of the ilmenite prior to the TGA experiments was 27.8 g kg^{-1} (Na + K), and 4.6 wt% and 10.3 wt% of the available alkali content was thus released in the inert and oxidizing atmospheres, respectively, under the present conditions.

The TGA-SID setup was concluded to provide valuable new information about the alkali stability and kinetics on the used ilmenite bed particles under inert and oxidizing conditions at temperatures up to 1000 °C. Under isothermal conditions at 1000 °C, the mass and alkali release both decayed on a time scale of approximately 1000 s in an inert atmosphere, and were approximately five times slower in an oxidizing atmosphere, indicating changes in the sample properties depending on the oxidizing capacity of the surrounding gas. An interesting feature is the similarity between the decays in weight and alkali release under inert conditions, which suggests that they are related to the same changes in the sample properties. Note that the alkali loss was two orders of magnitude smaller than the total weight loss (2.6 µg of alkali desorbed and 200 µg mass was lost between 3000 and 5000 s in an inert atmosphere), and alkali release was thus not directly responsible for the observed loss in the sample weight.

Figure 8 shows the results for different amounts of ilmenite samples, ranging from 1.6 to 20.3 mg at a constant temperature of 1000 °C in N_2. Figure 8a shows the total amount of alkali released by each sample during 90 min. Although some variations were seen, the results showed that the amount of released alkali did not have a significant dependence on the sample size, with an average amount of 0.28 µg alkali mg^{-1} sample. Figure 8b shows the corresponding alkali desorption profiles for each sample as a function of time. The profiles showed only small variations for sample sizes between 1.6 and 12.6 mg, whereas a deviation was seen for the largest sample of 20.3 mg. The observed change in kinetics is likely to be associated with the alkali desorption and re-adsorption processes within the ilmenite bed of particles when a relatively large sample is used. Although the absolute intensity of the alkali concentration changed with sample size, the relative intensity was concluded to have a linear dependence on the particle size.

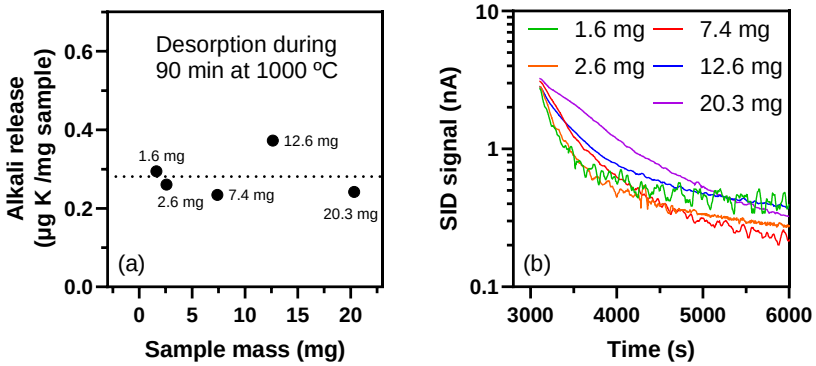

Figure 8. (**a**) Normalized amount of alkali released (µg mg^{-1} sample) as a function of the ilmenite sample size. The experiments were carried out during 90 min at a constant temperature of 1000 °C in N_2. The average alkali release of 0.28 µg alkali mg^{-1} sample is marked (dotted line). (**b**) Alkali desorption profiles with logarithmic SID intensities as a function of time.

4. Discussion

The experimental and modeling results showed that the TGA-SID method shares common challenges with other high temperature applications involving alkali compounds including the interactions of alkali in molecular and particulate forms with any of the present surfaces. The present study indicates that these challenges can be overcome based on the careful consideration of the conditions prevailing in different parts of the setup.

The observed alkali particle losses in cold exhaust tubes can qualitatively be understood based on well-known aerosol science concepts. The rapid cooling after leaving the TGA resulted in nucleation and the formation of new aerosol particles. Nucleation and the growth of aerosol particles during cooling typically resulted in particle number concentrations in the range 10^8–10^9 cm^{-3} [24]. Assuming that 5×10^8 cm^{-3} particles were formed and considering the measured alkali concentration ranges, the typical particle diameter ranges were estimated to be 8–19 nm in the biomass pyrolysis experiments and to 3–10 nm in the ilmenite experiments. The corresponding particle sizes in the case of experiments with pure salts may exceed 50 nm for the highest alkali amounts. The losses of particles should be negligible for large particles [24], but need to be considered for particles sizes below 20 nm, as illustrated by the experiments with ilmenite samples (Figure 4).

The transport time from the TGA to the SID was approximately 0.8 s for tubes with standard lengths, which was reduced to 0.2 s with the shortest tubes used here. Particles may continue to grow by agglomeration during their transport to the TGA. The agglomeration kinetics depend on the particle size and can be expected to be fast for sizes below 10 nm [24]. Small particles also grow faster than large ones and agglomeration may lead to the growth of particles to similar sizes for different alkali concentrations. This may potentially explain why the relative alkali signal does not depend on the alkali concentration (Figure 8), and further studies of the growth and loss of particles with sizes below 10 nm in the exhaust system would be valuable to confirm this.

The modeled loss of alkali compounds to the hot exhaust tube was large and consistent with the experimental results. This conclusion was based on the assumption that all alkali reaching the hot wall stuck to the hot surface and remained trapped on the time scale of the experiments. Extensive research on the interaction between alkali and quartz or other silica-containing materials showed that the alkali uptake was efficient and resulted in the formation of stable alkali–silicate compounds [7,9,43,44]. These earlier studies support the assumption made in the present study that alkali compounds that reach the hot quartz wall will remain bound to the surface. Although not studied in detail, this should also be valid for any alkali reaching the wall of the main TGA quartz reactor.

The experiments with pure alkali salts showed average losses of 26–39% for NaCl and KCl in the experimental system. The alkali concentrations were relatively high in this case, which led to the formation of large particles in the cold exhaust line and limited losses to

the walls. The observed losses are therefore likely to be dominated by losses to hot surfaces within the TGA.

The alkali concentrations were two orders of magnitude lower in the ilmenite and biomass studies, which may be considered representative for typical TGS-SID experiments. In these cases, the losses of both the molecular alkali compounds to hot surfaces and losses of formed aerosol particles to the cold exhaust tubes need to be considered. The KPS method suggests 25% transmission of alkali molecules in the hot areas. The results for the cold sampling lines in Figure 4 suggest that a 3 cm metal tube and a 7 cm rubber tube would result in a 80^{+18}_{-15}% transmission. If these results are combined, the total alkali transmission between the TGA and the SID would be 20^{+5}_{-4}% if the system is operated with the shortest exhaust tubes used here.

The present study used a standard TGA setup. A possible future line of development may be to evaluate alternative designs of the TGA and optimize the setup to reduce the losses of condensable material within the instrument. A starting point for this optimization is provided by the results from the KPS model concerning the hot exhaust line [36], and further studies should systematically investigate the influence of flow rate, tube material, tube length, and inner diameter to minimize the alkali losses.

The concept presented here may also be developed and extended by the use of other sensitive on-line instruments. A recent study presented an alternative SID concept that may distinguish between potassium and sodium based on differences in their desorption rate on a hot Pt filament [31]. Other potential on-line instruments with sufficient sensitivity for the present application include mass spectrometers for both organic [45] and inorganic compounds [46].

5. Conclusions

A TGA-SID instrument for laboratory studies of materials used in thermal conversion processes was developed and demonstrated. The method employs standard TGA and SID instruments that are combined to simultaneously characterize alkali release and mass loss from the materials used in thermal conversion processes.

The TGA-SID method relies on an understanding of alkali loss processes in the experimental setup. Alkali compounds nucleate to form nanometer-sized aerosol particles during extraction and quenching of the exhaust gas from the TGA. The losses of these particles to the walls of the sampling lines by diffusion may be significant, but can be understood and accounted for based on fundamental aerosol science. Losses of alkali in molecular form to hot walls within the TGA were evaluated using a molecular diffusion model and found to also be substantial. The experimental observations of losses are consistent with estimates based on modeling. Overall, the different types of losses cause uncertainties in absolute alkali concentrations, while uncertainties in relative alkali concentrations are substantially smaller. The technique was concluded to be well suited for the characterization of alkali emissions as a function of temperature and kinetics studies under isothermal conditions.

The operation of the instrument was demonstrated using biomass and fluidized bed material samples from an industrial process. The emissions of the alkali compounds during sample heating and isothermal conditions were determined and related to the simultaneous thermogravimetric analysis. The method was concluded to provide information on the connection between the alkali release and decomposition processes during biomass pyrolysis, and the alkali stability and kinetics on used ilmenite bed particles under inert and oxidizing conditions.

The new instrument was concluded to be a valuable complement to methods based on batch sampling, which provide detailed information about the alkali interactions with solid materials but have limited time resolution and therefore provide limited information about the kinetics. The TGA-SID method is robust and should be a useful tool for research purposes and studies of a variety of materials of interest in high temperature applications.

Supplementary Materials: The following supporting information can be downloaded at: https://www.mdpi.com/article/10.3390/en15124365/s1, Figure S1: Schematic overview of the experimental set-up used for calibration of the surface ionization detector (SID). KCl aerosol particles are generated with an aerosol atomizer (Model 3076, TSI Inc., Shoreview, MN, USA) and simultaneously fed to the SID and a scanning mobility particle sizer (SMPS; Model 3936, TSI Inc., Shoreview, MN, USA). Figure S2: Resulting gas velocity as vectors from CFD simulations of the TGA when operated at a constant temperature of 1000 °C in air. The 11 mm wide sample holder can be used as a reference for dimensions.

Author Contributions: Conceptualization, V.A., X.K. and J.B.C.P.; Methodology, V.A. and J.B.C.P.; Formal analysis, V.A.; Investigation, V.A., Y.G., X.K. and J.B.C.P.; Resources, J.B.C.P.; Data curation, V.A.; Writing—original draft preparation, V.A. and J.B.C.P.; Writing—review and editing, V.A., Y.G., X.K. and J.B.C.P.; Supervision, X.K. and J.B.C.P.; Project administration, J.B.C.P.; Funding acquisition, J.B.C.P. All authors have read and agreed to the published version of the manuscript.

Funding: This research was funded by the Swedish Research Council, project "Biomass combustion chemistry with oxygen carriers" 2016-06023. This work was carried out within the Swedish Gasification Centre consortium.

Data Availability Statement: Not applicable.

Conflicts of Interest: The authors declare no conflict of interest.

References

1. Zhang, L.; Xu, C.; Champagne, P. Overview of recent advances in thermo-chemical conversion of biomass. *Energy Convers. Manag.* **2010**, *51*, 969–982. [CrossRef]
2. Khan, A.A.; de Jong, W.; Jansens, P.J.; Spliethoff, H. Biomass combustion in fluidized bed boilers: Potential problems and remedies. *Fuel Process. Technol.* **2009**, *90*, 21–50. [CrossRef]
3. Zevenhoven, M.; Yrjas, P.; Hupa, M. Ash-Forming Matter and Ash-Related Problems. In *Handbook of Combustion*; WILEY-VCH: Weinheim, Germany, 2010; Volume 4.
4. Wang, C.A.; Jin, X.; Wang, Y.; Yan, Y.; Cui, J.; Liu, Y.; Che, D. Release and Transformation of Sodium during Pyrolysis of Zhundong Coals. *Energy Fuels* **2015**, *29*, 78–85. [CrossRef]
5. Andersson, V.; Soleimanisalim, A.H.; Kong, X.; Leion, H.; Mattisson, T.; Pettersson, J.B.C. Alkali interactions with a calcium manganite oxygen carrier used in chemical looping combustion. *Fuel Process. Technol.* **2022**, *227*, 107099. [CrossRef]
6. Corcoran, A.; Knutsson, P.; Lind, F.; Thunman, H. Mechanism for Migration and Layer Growth of Biomass Ash on Ilmenite Used for Oxygen Carrier Aided Combustion. *Energy Fuels* **2018**, *32*, 8845–8856. [CrossRef]
7. Staničić, I.; Andersson, V.; Hanning, M.; Mattisson, T.; Backman, R.; Leion, H. Combined manganese oxides as oxygen carriers for biomass combustion—Ash interactions. *Chem. Eng. Res. Des.* **2019**, *149*, 104–120. [CrossRef]
8. Störner, F.; Hildor, F.; Leion, H.; Zevenhoven, M.; Hupa, L.; Rydén, M. Potassium Ash Interactions with Oxygen Carriers Steel Converter Slag and Iron Mill Scale in Chemical-Looping Combustion of Biomass—Experimental Evaluation Using Model Compounds. *Energy Fuels* **2020**, *34*, 2304–2314. [CrossRef]
9. Öhman, M.; Nordin, A.; Skrifvars, B.-J.; Backman, R.; Hupa, M. Bed Agglomeration Characteristics during Fluidized Bed Combustion of Biomass Fuels. *Energy Fuels* **2000**, *14*, 169–178. [CrossRef]
10. Corcoran, A.; Marinkovic, J.; Lind, F.; Thunman, H.; Knutsson, P.; Seemann, M. Ash Properties of Ilmenite Used as Bed Material for Combustion of Biomass in a Circulating Fluidized Bed Boiler. *Energy Fuels* **2014**, *28*, 7672–7679. [CrossRef]
11. Hildor, F.; Zevenhoven, M.; Brink, A.; Hupa, L.; Leion, H. Understanding the Interaction of Potassium Salts with an Ilmenite Oxygen Carrier Under Dry and Wet Conditions. *ACS Omega* **2020**, *5*, 22966–22977. [CrossRef]
12. Staničić, I.; Hanning, M.; Deniz, R.; Mattisson, T.; Backman, R.; Leion, H. Interaction of oxygen carriers with common biomass ash components. *Fuel Process. Technol.* **2020**, *200*, 106313. [CrossRef]
13. Gogolev, I.; Linderholm, C.; Gall, D.; Schmitz, M.; Mattisson, T.; Pettersson, J.B.C.; Lyngfelt, A. Chemical-looping combustion in a 100 kW unit using a mixture of synthetic and natural oxygen carriers—Operational results and fate of biomass fuel alkali. *Int. J. Greenh. Gas Control* **2019**, *88*, 371–382. [CrossRef]
14. Moud, P.H.; Andersson, K.J.; Lanza, R.; Pettersson, J.B.C.; Engvall, K. Effect of gas phase alkali species on tar reforming catalyst performance: Initial characterization and method development. *Fuel* **2015**, *154*, 95–106. [CrossRef]
15. Yu, J.; Guo, Q.; Gong, Y.; Ding, L.; Wang, J.; Yu, G. A review of the effects of alkali and alkaline earth metal species on biomass gasification. *Fuel Process. Technol.* **2021**, *214*, 106723. [CrossRef]
16. Mitsuoka, K.; Hayashi, S.; Amano, H.; Kayahara, K.; Sasaoaka, E.; Uddin, M.A. Gasification of woody biomass char with CO_2: The catalytic effects of K and Ca species on char gasification reactivity. *Fuel Process. Technol.* **2011**, *92*, 26–31. [CrossRef]
17. Gyllén, A.; Knutsson, P.; Lind, F.; Thunman, H. Magnetic separation of ilmenite used as oxygen carrier during combustion of biomass and the effect of ash layer buildup on its activity and mechanical strength. *Fuel* **2020**, *269*, 117470. [CrossRef]

18. Gall, D.; Pushp, M.; Davidsson, K.O.; Pettersson, J.B.C. Online Measurements of Alkali and Heavy Tar Components in Biomass Gasification. *Energy Fuels* **2017**, *31*, 8152–8161. [CrossRef]
19. Gall, D.; Pushp, M.; Larsson, A.; Davidsson, K.; Pettersson, J.B.C. Online Measurements of Alkali Metals during Start-up and Operation of an Industrial-Scale Biomass Gasification Plant. *Energy Fuels* **2018**, *32*, 532–541. [CrossRef]
20. Andersson, V.; Soleimanisalim, A.H.; Kong, X.; Hildor, F.; Leion, H.; Mattisson, T.; Pettersson, J.B.C. Alkali-wall interactions in a laboratory-scale reactor for chemical looping combustion studies. *Fuel Process. Technol.* **2021**, *217*, 106828. [CrossRef]
21. Porbatzki, D.; Stemmler, M.; Müller, M. Release of inorganic trace elements during gasification of wood, straw, and miscanthus. *Biomass Bioenergy* **2011**, *35*, S79–S86. [CrossRef]
22. Erbel, C.; Mayerhofer, M.; Monkhouse, P.; Gaderer, M.; Spliethoff, H. Continuous in situ measurements of alkali species in the gasification of biomass. *Proc. Combust. Inst.* **2013**, *34*, 2331–2338. [CrossRef]
23. Sepman, A.; Ögren, Y.; Qu, Z.; Wiinikka, H.; Schmidt, F.M. Real-time in situ multi-parameter TDLAS sensing in the reactor core of an entrained-flow biomass gasifier. *Proc. Combust. Inst.* **2017**, *36*, 4541–4548. [CrossRef]
24. Hinds, W.C. *Aerosol Technology—Properties, Behavior and Measurement of Airborne Particles*; Wiley: New York, NY, USA, 1999.
25. Olsson, J.G.; Jäglid, U.; Pettersson, J.B.C.; Hald, P. Alkali Metal Emission during Pyrolysis of Biomass. *Energy Fuels* **1997**, *11*, 779–784. [CrossRef]
26. Davidsson, K.O.; Stojkova, B.J.; Pettersson, J.B.C. Alkali Emission from Birchwood Particles during Rapid Pyrolysis. *Energy Fuels* **2002**, *16*, 1033–1039. [CrossRef]
27. Hagström, M.; Engvall, K.; Pettersson, J.B.C. Desorption Kinetics at Atmospheric Pressure: Alkali Metal Ion Emission from Hot Platinum Surfaces. *J. Phys. Chem. B* **2000**, *104*, 4457–4462. [CrossRef]
28. Davidsson, K.; Engvall, K.; Hagström, M.; Korsgren, J.; Lönn, B.; Pettersson, J. A Surface Ionization Instrument for On-Line Measurements of Alkali Metal Components in Combustion: Instrument Description and Applications. *Energy Fuels* **2002**, *16*, 1369–1377. [CrossRef]
29. Gogolev, I.; Soleimanisalim, A.H.; Linderholm, C.; Lyngfelt, A. Commissioning, performance benchmarking, and investigation of alkali emissions in a 10 kWth solid fuel chemical looping combustion pilot. *Fuel* **2021**, *287*, 119530. [CrossRef]
30. Pushp, M.; Gall, D.; Davidsson, K.; Seemann, M.; Pettersson, J.B.C. Influence of Bed Material, Additives, and Operational Conditions on Alkali Metal and Tar Concentrations in Fluidized Bed Gasification of Biomass. *Energy Fuels* **2018**, *32*, 6797–6806. [CrossRef]
31. Gall, D.; Nejman, C.; Allguren, T.; Andersson, K.; Pettersson, J.B.C. A new technique for real-time measurements of potassium and sodium aerosols based on field-reversal surface ionization. *Meas. Sci. Technol.* **2021**, *32*, 075802. [CrossRef]
32. Moldenhauer, P.; Gyllén, A.; Thunman, H.; Lind, F. A Scale-Up Project for Operating a 115 MWth Biomass-Fired CFB boiler with Oxygen Carriers as Bed Material. In Proceedings of the 5th International Conference on Chemical Looping, Park City, UT, USA, 24–27 September 2018.
33. Gosiewski, K.; Pawlaczyk-Kurek, A. Aerodynamic CFD simulations of experimental and industrial thermal flow reversal reactors. *Chem. Eng. J.* **2019**, *373*, 1367–1379. [CrossRef]
34. Pashchenko, D.I. CFD Modeling of Operating Processes of a Solar Air Heater in ANSYS FLUENT. *J. Eng. Phys. Thermophys.* **2019**, *92*, 73–79. [CrossRef]
35. Li, S.; Shen, Y. An approach to simulate gas-solid flow systems with process controllers. *Chem. Eng. J.* **2022**, *429*, 132443. [CrossRef]
36. Knopf, D.A.; Pöschl, U.; Shiraiwa, M. Radial Diffusion and Penetration of Gas Molecules and Aerosol Particles through Laminar Flow Reactors, Denuders, and Sampling Tubes. *Anal. Chem.* **2015**, *87*, 3746–3754. [CrossRef] [PubMed]
37. Mostinsky, I.L. Diffusion Coefficient. Available online: https://www.thermopedia.com/content/696/ (accessed on 18 November 2021).
38. Diffusion Coefficient. Available online: https://www.comsol.com/multiphysics/diffusion-coefficient (accessed on 18 November 2021).
39. Idris, S.S.; Rahman, N.A.; Ismail, K.; Alias, A.B.; Rashid, Z.A.; Aris, M.J. Investigation on thermochemical behaviour of low rank Malaysian coal, oil palm biomass and their blends during pyrolysis via thermogravimetric analysis (TGA). *Bioresour. Technol.* **2010**, *101*, 4584–4592. [CrossRef] [PubMed]
40. White, J.E.; Catallo, W.J.; Legendre, B.L. Biomass pyrolysis kinetics: A comparative critical review with relevant agricultural residue case studies. *J. Anal. Appl. Pyrolysis* **2011**, *91*, 1–33. [CrossRef]
41. Çepelioğullar, Ö.; Pütün, A.E. Thermal and kinetic behaviors of biomass and plastic wastes in co-pyrolysis. *Energy Convers. Manag.* **2013**, *75*, 263–270. [CrossRef]
42. Kowalski, T.; Ludwig, C.; Wokaun, A. Qualitative Evaluation of Alkali Release during the Pyrolysis of Biomass. *Energy Fuels* **2007**, *21*, 3017–3022. [CrossRef]
43. Gogolev, I.; Pikkarainen, T.; Kauppinen, J.; Linderholm, C.; Steenari, B.-M.; Lyngfelt, A. Investigation of biomass alkali release in a dual circulating fluidized bed chemical looping combustion system. *Fuel* **2021**, *297*, 120743. [CrossRef]
44. Faust, R.; Berdugo Vilches, T.; Malmberg, P.; Seemann, M.; Knutsson, P. Comparison of Ash Layer Formation Mechanisms on Si-Containing Bed Material during Dual Fluidized Bed Gasification of Woody Biomass. *Energy Fuels* **2020**, *34*, 8340–8352. [CrossRef]

45. Yatavelli, R.L.N.; Lopez-Hilfiker, F.; Wargo, J.D.; Kimmel, J.R.; Cubison, M.J.; Bertram, T.H.; Jimenez, J.L.; Gonin, M.; Worsnop, D.R.; Thornton, J.A. A Chemical Ionization High-Resolution Time-of-Flight Mass Spectrometer Coupled to a Micro Orifice Volatilization Impactor (MOVI-HRToF-CIMS) for Analysis of Gas and Particle-Phase Organic Species. *Aerosol Sci. Technol.* **2012**, *46*, 1313–1327. [CrossRef]
46. Pratt, K.A.; Prather, K.A. Mass spectrometry of atmospheric aerosols—Recent developments and applications. Part II: On-line mass spectrometry techniques. *Mass Spectrom. Rev.* **2012**, *31*, 17–48. [CrossRef] [PubMed]